

VIP Very Important Paper

CHEM
BIO
TALENTS

A Promiscuous Cytochrome P450 Hydroxylates Aliphatic and Aromatic C–H Bonds of Aromatic 2,5-Diketopiperazines

Guangde Jiang,^[a] Yi Zhang,^[a] Magan M. Powell,^[a] Sarah M. Hylton,^[a] Nicholas W. Hiller,^[a] Rosemary Loria,^[b] and Yousong Ding^{*[a]}

Cytochrome P450 enzymes generally functionalize inert C–H bonds, and thus, they are important biocatalysts for chemical synthesis. However, enzymes that catalyze both aliphatic and aromatic hydroxylation in the same biotransformation process have rarely been reported. A recent biochemical study demonstrated the P450 TxtC for the biosynthesis of herbicidal thaxtomins as the first example of this unique type of enzyme. Herein, the detailed characterization of substrate requirements and biocatalytic applications of TxtC are reported. The results

reveal the importance of N-methylation of the thaxtomin diketopiperazine (DKP) core on enzyme reactions and demonstrate the tolerance of the enzyme to modifications on the indole and phenyl moieties of its substrates. Furthermore, hydroxylated, methylated, aromatic DKPs are synthesized through a biocatalytic route comprising TxtC and the promiscuous *N*-methyltransferase Amir_4628; thus providing a basis for the broad application of this unique P450.

Introduction

Cytochrome P450 enzymes (P450s) are a superfamily of monooxygenases that are exploited in all kingdoms of life to execute a broad array of physiological functions, for example, xenobiotic metabolism and metabolite synthesis.^[1] These heme–thiolate proteins generally use O₂ and a reducing cofactor, NAD(P)H, to insert one oxygen atom into an organic substrate, often the inert C–H bond, leading to hydroxylation and epoxidation reactions, as well as tens of less common reactions (e.g., aryl coupling and molecular rearrangement).^[2] The catalytic mechanism of P450s has been extensively studied over past decades.^[3] The primary reactive intermediate driving P450 reactions is one porphyrin π -radical cation ferryl species, known as compound I,^[3b,4] which abstracts a hydrogen atom from the substrate to yield both compound II (an Fe⁴⁺–OH species) and a substrate radical species. The latter rebinds to the hydroxyl radical of compound II to generate a hydroxylated product. In addition to compound I, nature has exploited other reactive species of the P450 catalytic cycle (e.g., ferric peroxo and/or

hydroperoxo species) for chemical innovations.^[5] The ability to functionalize inert C–H bonds of an extraordinarily broad range of substrates in a regio- and stereospecific manner makes P450s valuable to a variety of synthetic applications.^[6]

Natural products and their synthetic derivatives have countless applications in medicine, veterinary practice, agriculture, and industry.^[7] These compounds occupy enormously broad structural diversity, presumably translating into their impressive functional richness.^[8] P450s are key players to bestow and expand the structural diversity of natural products.^[1b,2b,9] Indeed, they can diversify building blocks for the assembly of natural products and modify assembled intermediates for the attachment of additional moieties or interactions with other targets. Accommodating a tremendously wide substrate range and a broad reaction scope, P450s involved in natural product biosynthesis have evolved with many intriguing features.^[1b,2b,9] In particular, some P450s catalyze multiple transformations in the same biosynthetic pathway (Scheme 1). For example, PikC hydroxylates C10 and C12 of the 12-membered polyketide (PK) macrolide YC-17 and C12 and C14 of 14-membered narbomycin in the antibiotic pikromycin/methymycin biosynthetic pathway,^[10] whereas TamI catalyzes at least three oxidation reactions on three sites to produce the PK/nonribosomal peptide (NRP) hybrid antibiotic tirandamycin (Scheme 1A).^[11] Similarly, P450_{sky} hydroxylates the β position of three amino acid building blocks tethered onto the corresponding thiolation domains in the biosynthesis of NRP skyllamycin (Scheme 1A).^[12] Modifications on multiple sites by a single P450 are also important for the biosynthesis of other families of natural products, for example, Tri4 in tailoring the terpenoid mycotoxin trichodiene^[13] and TsrR for the production of the ribosomally synthesized and post-translationally modified peptide antibiotic thio-

[a] G. Jiang, Y. Zhang, M. M. Powell, S. M. Hylton, N. W. Hiller, Prof. Y. Ding
Department of Medicinal Chemistry
Center for Natural Products, Drug Discovery and Development
University of Florida
Gainesville, FL 32610 (USA)
E-mail: yding@cop.ufl.edu

[b] Prof. R. Loria
Department of Plant Pathology
Institute of Food and Agricultural Sciences, University of Florida
Gainesville, FL 32611 (USA)

Supporting information and the ORCID identification numbers for the authors of this article can be found under <https://doi.org/10.1002/cbic.201800736>.

This article is part of the young researchers' issue ChemBioTalents. To view the complete issue, visit <http://chembiochem.org/chembiotalents>

strepton (Scheme 1A).^[14] Notably, multifunctional P450s are also found in primary metabolism pathways, as exemplified by CYP11A, CYP17, and CYP11B2 in the biosynthesis of steroid hormones;^[15] CYP107H1 (P450_{Biol}) in the formation of pimelic acid as the majority of the carbon skeleton of biotin;^[16] and CYP24A1 in the degradation of vitamin D.^[17] On the other hand, many natural products have a high abundance of aromatic and aliphatic C–H bonds, but it is rarely known for any biosynthetic P450 to catalyze both aromatic and aliphatic hydroxylation.^[18] The dissociation energy of these two types of C–H bonds is different by about 10 to 20 kcal mol⁻¹. To address this energy difference, P450s usually employ the hydrogen abstraction strategy by using compound I for aliphatic hydroxylation, while generating an initial epoxide ring followed by a 1,2-hydride shift for the formation of the aromatic C–OH group.^[3,19] Notably, both reactions are well within the range of P450 activities (Scheme 1A),^[3] but rarely catalyzed by any single enzyme.

Thaxtomins are virulence factors of multiple plant pathogenic *Streptomyces* strains and cause potato common scab disease.^[20] Two NRP synthetases (NRPSs), TxtA and TxtB, assemble L-phenylalanine (L-Phe) and 4-NO₂-L-tryptophan (4NO₂-L-Trp) into one 2,5-diketopiperazine (DKP) thaxtomin D (**3**; Scheme 1B).^[20,21] 4NO₂-L-Trp is converted from L-Trp by a unique P450 TxtE that uses cosubstrates O₂ and nitric oxide synthesized from L-arginine by TxtD.^[20,22] Genetic studies of thaxtomin biosynthesis imply that the second pathway-specific P450 TxtC sequentially hydroxylates the aliphatic tertiary C14 and aromatic C20 of **3** to produce thaxtomins B (**2**) and A (**1**; Scheme 1B).^[21b,23] Recently, we biochemically confirmed the dual functions of recombinant TxtC fused with the reductase domain of P450BM3 (BM3R) through a 14-amino acid linker, named as TCB14.^[21a] In addition, we revealed substantial substrate promiscuity of TCB14 toward nitro-containing thaxtomins in aliphatic and aromatic hydroxylation as the biocatalytic production of 58 hydroxylated thaxtomin analogues from 3 L-Trp and 12 L-Phe analogues.^[21a] This work provides the first biochemical evidence for the existence of natural P450s for both aliphatic and aromatic C–H hydroxylation, which is further supported by a recent report on the structural characteri-

zation of TxtC.^[24] The only other known example is the P450 FmoC/TbrH, which hydroxylates both the indole ring and the β position of 6-chlorotryptophan attached to the thiolation domain in genetic studies on the biosynthesis of JBIR-34/35/tambromycin (Scheme 1A).^[18] The DKP core is a privileged scaffold in drug research,^[25] and selective hydroxylation of the core by chemical methods is lengthy and sometimes synthetically challenging.^[26] So far, only three P450s, CYP121, CYP134A1, and BcmD, are known to be involved in the biosynthesis of DKP natural products mycocyclosin,^[27] pulcherrimic acid,^[28] and bicyclomycin,^[29] respectively (Scheme 1A).

Herein, we describe the further development of TxtC as a biocatalyst for hydroxylating aromatic DKPs. We first engineered the linker length between TxtC and BM3R and found TCB14 as the most active variant among four fusion enzymes toward **3**. By using **3**, thaxtomin C (**4**), and two unnatural analogues (**5**, **6**) as substrates (Scheme 1B), we observed the significant effects of N-methylations of the DKP core on the reactivity and product profiles of TCB14. The substrate scope of TCB14 was further evaluated with 30 desnitro thaxtomin analogues synthesized from 5 L-Trp and 6 L-Phe analogues by TxtA and TxtB, yielding 43 hydroxylated desnitro thaxtomin analogues. Finally, we developed one new biocatalytic route by using TCB14 and one promiscuous N-methyltransferase (MT) Amir_4628 from the actinobacterium *Actinosynnema mirum*^[30] along with the human methionine adenosyltransferase (hMAT2A),^[31] which forms S-adenosylmethionine (SAM) from L-methionine and ATP, and successfully synthesized several hydroxylated di-N-methylated aromatic DKPs.

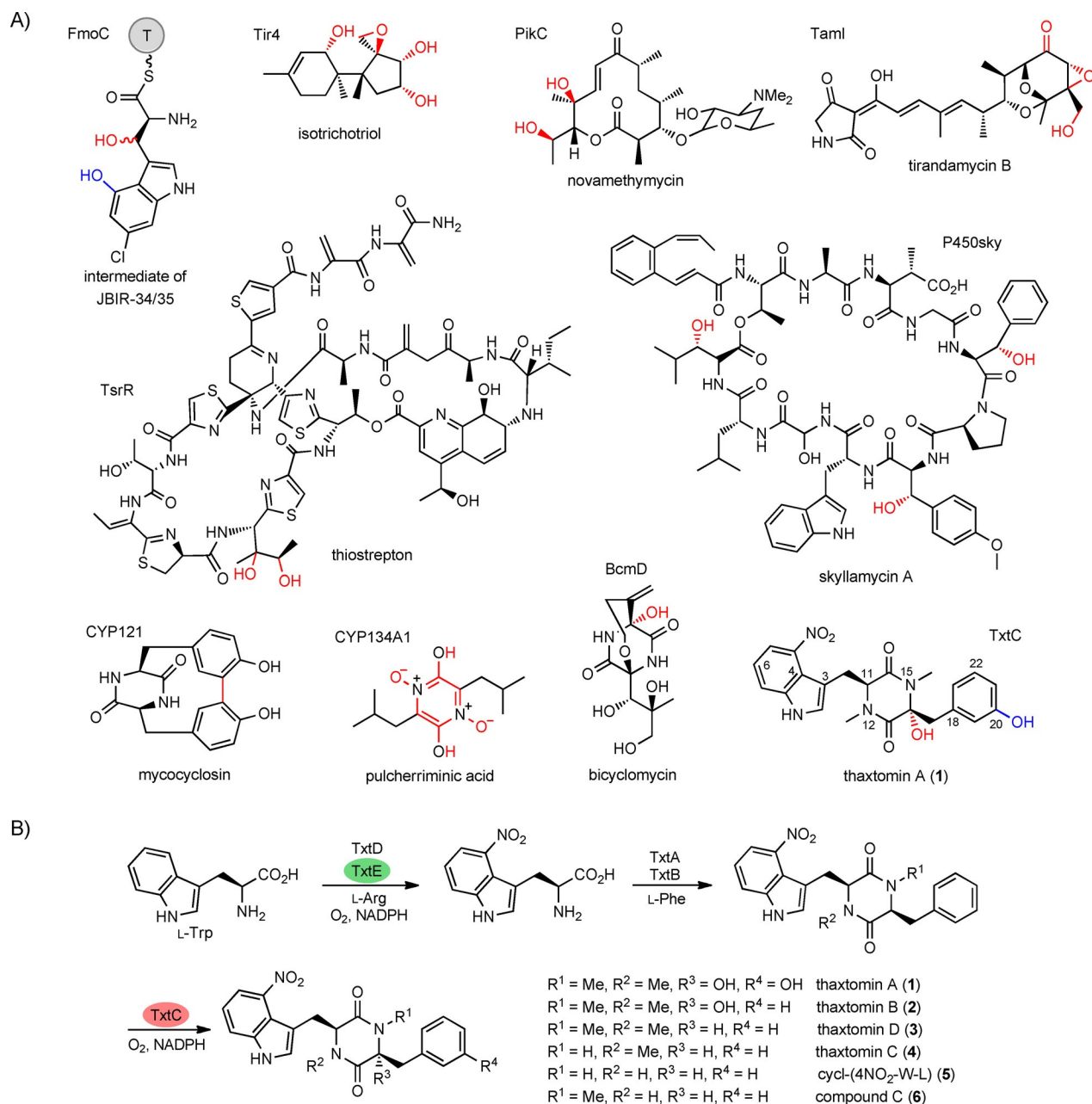
Results and Discussion

Effect of the linker length between TxtC and BM3R on the catalytic activity of fusion enzymes

P450 reactions generally require redox partners to shuttle electrons from the reducing agent. In a previous study, we created 15 self-sufficient TxtE nitration biocatalysts by fusing the P450 with BM3R through linkers of 3 to 27 amino acids,^[32] easing biocatalytic use. Notably, the natural linker sequence between the P450BM3 heme domain and BM3R was used to create chimeric enzymes that were named TBX, in which X corresponded to the linker length. Among these fusion enzymes, TB14 demonstrates the highest activity in nitrating L-Trp, whereas TB3, TB6, and TB9 are not properly folded and inactive. Recently, we used the same design to create self-sufficient TCB14, which was highly soluble and catalytically active toward 32 analogues of thaxtomin D (**3**).^[21a] To identify highly active TxtC biocatalysts for DKP hydroxylation, we sought to examine the potential effect of the linker length on the catalytic performance of chimeric TxtC–BM3R fusion enzymes. Following the previous protocol, we created chimeric TCB11, TCB17, and TCB22 with linkers of 11, 17, and 22 amino acids, respectively (Figure 1A). All variants were expressed as soluble proteins in *Escherichia coli* and possessed featured Soret bands at $\lambda = 450$ nm in their differential CO-reduced spectra (Figures S1 and S2 in the Supporting Information). We then incubated 1.5 μ M recombinant

Yousong Ding received his Ph.D. from the University of Michigan, Ann Arbor, where he studied the biosynthesis and chemoenzymatic synthesis of microbial natural products in the group of Prof. David Sherman. In 2010, Yousong started his postdoctoral studies on biocatalysis and synthetic biology with Prof. Frances Arnold at the California Institute of Technology. After a short period with Pfizer, Yousong began his independent career as an assistant professor of Medicinal Chemistry at the University of Florida, Gainesville, in 2013. His group focuses on the discovery and development of bioactive substances from natural resources.





Scheme 1. A) Selected examples of multifunctional P450s discussed in this study. TxtC and FmoC are unique in catalyzing both aliphatic (red) and aromatic (blue) hydroxylation. Notably, TamI works along with TamL to form the ketone of tirandamycin B labeled in red. B) Schematic outline of the thaxtomin biosynthetic pathway. Chemical structures of natural and unnatural thaxtomin analogues 1–6 are also shown.

enzymes and the glucose dehydrogenase (GDH)-based NADPH regeneration system with 0.1 mM **3** as a substrate for 2 h.^[21a] HPLC analysis revealed the production of **2** in all reactions, and TCB14 was the most active enzyme, followed by TCB11 and TCB17 (73.5 and 55.7% of the activity of TCB14, respectively; Figure 1B). The catalytic performance of these self-sufficient enzymes was presumably determined by their coupling efficiency. The highest coupling efficiency was observed with TCB14 ((2.36 ± 0.08)%), followed by TCB11 ((1.98 ± 0.15)%), TCB17 ((1.87 ± 0.14)%), and TCB22 ((1.38 ± 0.07)%). On the other hand, the low coupling efficiency of these enzymes suggests an important direction for the future development of

TxtC as biocatalysts. Nonetheless, TCB14 was used to gain useful insights into its substrate scope in the following studies.

Influence of N-methylation of thaxtomin substrates on the reactivity and product profile of TCB14

Plant pathogenic *Streptomyces* strains produce 12 known thaxtomin analogues, the structures of which mainly differ in N-methylation of the DKP scaffold and hydroxylation on the phenyl group of L-Phe.^[20] The N12- and N15-CH₃ groups are installed by the MT domain of NRPS TxtB and TxtA, respectively, whereas TxtC hydroxylates the phenyl group as one of its

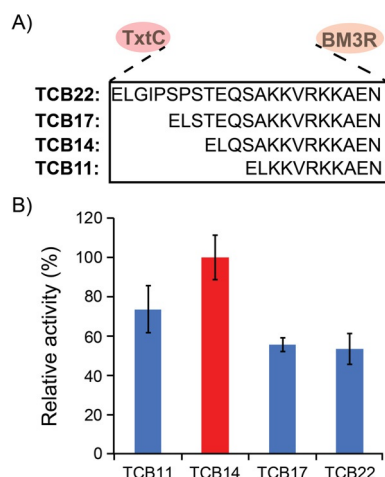


Figure 1. TCB14 was the most active among four self-sufficient chimeric enzymes. A) Schematic illustration of four self-sufficient chimeric enzymes, including linker sequences. B) The relative activities of four chimeric enzymes. The reactions contained 1.5 μM enzyme and 0.1 mM **3** and were terminated after 2 h. The amount of **2** in the reaction mixtures was determined at 380 nm through HPLC analysis. The amount of **2** in the TCB14 reaction was set as 100% to normalize the relative activities of other enzymes. The data represent means \pm standard deviation (s.d.) of at least two independent experiments.

two reactions (Scheme 1B). Our recent in vitro study revealed that the N-methylation of thaxtomins was controlled by the availability of SAM in TxtA and TxtB reactions.^[21a] If [SAM] is limiting, one thaxtomin analogue without any N-CH₃ group (**5**) is produced, along with small quantities of **3** and **4** carrying the N12-CH₃ group (Scheme 1B).^[21a] However, whether the N-methylation status of thaxtomin substrates influences the TxtC reactions is unknown. To address this question, we examined the performance of TCB14 toward **3**, **4**, **5**, and one unnatural thaxtomin analogue (**6**) that carried the single N15-CH₃ group (Scheme 1B). Compounds **3** and **4** were isolated from the culture medium of one thaxtomin-producing *Streptomyces albus-thx2* strain that we previously created,^[21b] whereas **5** was enzymatically synthesized in the reaction of TB14, TxtA, and TxtB without SAM.^[21a] To enzymatically synthesize **6**, we prepared recombinant TxtB G554R mutant in *E. coli* (Figure S1). The G₅₅₂XG₅₅₄XG₅₅₆ motif in TxtB MT is highly conserved among N-MTs of multiple NRPSs and essential for the binding of SAM (Figure S3).^[33] The G554R mutation is thus expected to inactivate the MT domain of TxtB. Indeed, we observed a single product from the reaction of TB14, TxtA, and TxtB G554R that showed an expected *m/z* value (393.1557, $\Delta 0.5$ ppm) through HRMS analysis (Figure 2A). The structure of compound **6** was further elucidated by means of 1D and 2D NMR spectroscopy analysis (Figures 2A and S4).

Having prepared **3–6**, we examined the catalytic performance of TCB14 toward these substrates. At 1.5 μM , TCB14 converted (13.0 \pm 1.4)% of **3** (0.1 mM) into **2** within 2 h (trace I, Figure 2B). By contrast, compound **5** was completely inactive in the reaction with TCB14 under the same conditions. Further incubation of the reaction containing ten times more TCB14 (15 μM) for 20 h led to undetectable amounts of hydroxylated

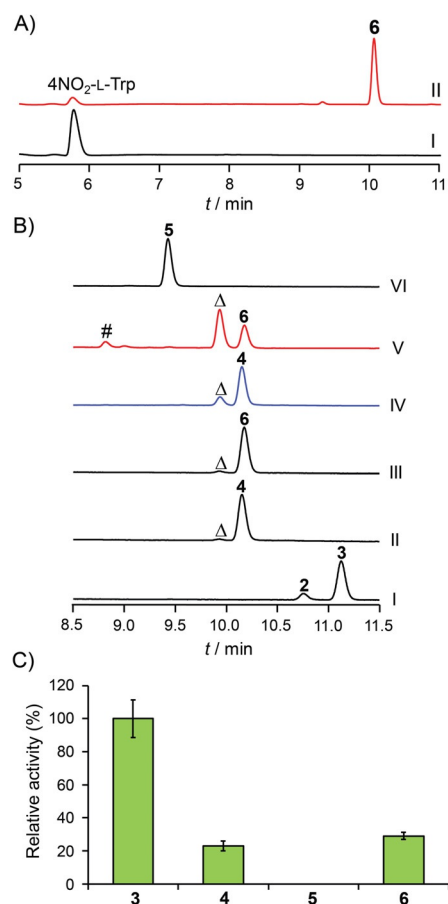


Figure 2. Characterization of the effects of substrate N-methylations on TCB14 performance. A) HPLC analysis revealed the production of **6** in the reaction of TB14, TxtA, and TxtB G554R (trace II), which was missing from the control carrying heat-inactivated TxtB G554R (trace I). B) HPLC analysis showed different product profiles of reactions of TCB14 with **3–6** as substrates. Traces I–III represent the reactions containing 1.5 μM TCB14 and 0.1 mM substrate for 2 h, whereas traces IV–VI show the reactions with 15 μM TCB14 and 0.2 mM substrate for 20 h. The peaks of monohydroxylated **4** and **6** are indicated with Δ , whereas # shows dihydroxylated **6**. C) The relative activities of TCB14 toward **3–6**. The amounts of monohydroxylated products in TCB14 reactions after 2 h were determined at 380 nm through HPLC analysis and the highest amount ((13.0 \pm 0.1) μM of **2**) was set as 100% to normalize the relative activities of the enzyme toward other substrates. The data represent means \pm s.d. of at least two independent experiments.

5 by means of HPLC and LC-MS analyses (trace VI, Figure 2B). On the other hand, TCB14 (1.5 μM) produced monohydroxylated **4** and **6** (0.1 mM substrate) after 2 h (traces II and III, Figure 2B). Both products showed expected *m/z* values in HRMS analysis and diagnostic tandem MS patterns that allowed accurate assignment of their structures (Figures S5 and S6 and Table S1).^[21a] This work further revealed **6** as the second best substrate of TCB14 in C14-hydroxylation, but only with (29.0 \pm 2.1)% relative activity of **3**, followed by **4** ((23.0 \pm 3.1)% relative activity of **3**; Figure 2C). The relative activities of these substrates agreed with the trend of their binding affinities with TCB14. Bi-layer interferometry (BLI) technology revealed the strongest interaction between **3** and TCB14 ($K_d = 33$ μM), which was in the same range of the K_m value ((30.0 \pm 6.2) μM) determined in our recent kinetic study,^[21a] followed by **6** and **4** ($K_d =$

0.14 and 1.1 mM, respectively). Compound **5** showed no measurable binding with TCB14. Strong binding between **3** and TCB14 ($K_d = (9.8 \pm 0.7) \mu\text{M}$) was confirmed by means of the UV titration method.^[32] Notably, the maximal absorbance of **3** is around 380 nm and has significant interference with the substrate-bound Soret band at around 392 nm. We further evaluated the catalytic performance of TCB14 toward two monomethylated substrates by incubating the reactions containing 15 μM of TCB14 and 0.2 mM of **4** and **6** for 20 h (Scheme 1B). HPLC analysis of the reactions revealed only monohydroxylated **4** (about 16% conversion) and about 75% conversion of **6** into 69% monohydroxylated and 6% dihydroxylated **6** (traces IV and V, Figure 2B and Table S1). These results together suggested that the N-CH₃ groups of the thaxtomin DKP core affect the substrate/enzyme interactions, thereby influencing the catalytic performance of TCB14. Recently, the group of Challis reported a **3**-bound TxtC crystal structure (PDB ID: 6F0B).^[24] In the range of 5 Å, Leu74, Val168, Val 169, and Val232 form a hydrophobic cavity for the binding of the N12-CH₃ group of **3**, whereas Leu284 and Thr384, along with Ser280, mediate interactions with N15-CH₃ (Figure S7). As such, the lack of both DKP N-CH₃ groups in **5** is likely to lead to no interactions with the hydrophobic pockets within the active site of TxtC. On the other hand, one DKP N-CH₃ group in **4** or **6** seems to be sufficient to mediate catalytically effective interactions (Figure 2), albeit with significantly lower catalytic performance than that of **3**.

Hydroxylation of 28 desnitro analogues of thaxtomin D (**3**) by TCB14

The structures of natural thaxtomins contain the C4-NO₂ group, which is important to their virulence activity (Scheme 1B).^[20] We recently revealed the promiscuity of TCB14 toward 32 nitro-containing thaxtomin analogues.^[21a] However, the extent to which the C4-NO₂ group influences the activity of TxtC has not been studied, to date; an advanced understanding would aid the development of this enzyme for biocatalytic uses. To tackle this question, we first synthesized desnitro-4Me-thaxtomin D (**7**) in reactions of TxtA and TxtB (1.2 μM) with 4Me-D,L-Trp (0.5 mM) and L-Phe (0.5 mM) as substrates. In our previous study, TxtA and TxtB were evaluated with five L-Trp and six L-Phe analogues, and the highest conversion ratio (about 22%) was observed with the above two substrates.^[21a] HPLC analysis revealed the successful synthesis of **7** with the same retention time as that of the standard (traces I and II, Figure 3A).^[21a] We then included TCB14 (4.5 μM) along with the regeneration system of NADPH in the reaction of TxtA and TxtB for an additional 20 h. Two new peaks with an increased polarity were observed by HPLC analysis (trace III, Figure 3A) and showed *m/z* values identical to those of mono- and dihydroxylated **7** (392.1960, $\Delta 2.3$ ppm; 408.1918, $\Delta 0.2$ ppm), which were further supported by their MS/MS fragmentation patterns (Table S2). Dihydroxylated **7** was the major product (about 75%) of the reaction. Notably, compound **7** produced in the TxtA and TxtB reaction (calculated to be 0.11 mM) was completely consumed by TCB14; thus indicating

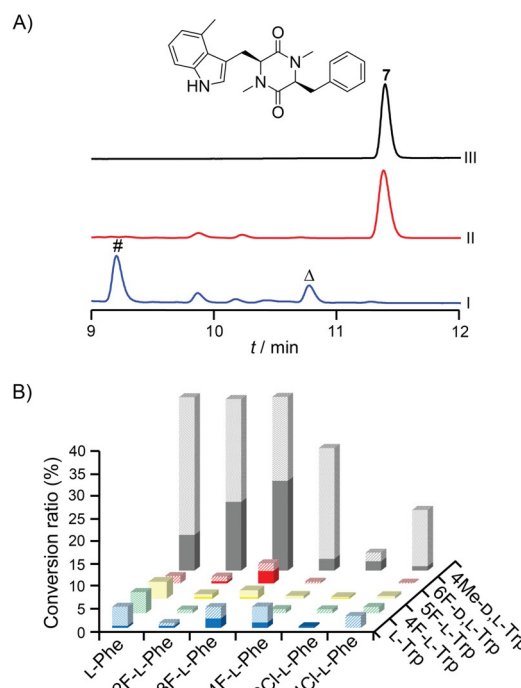


Figure 3. Biocatalytic synthesis of hydroxylated desnitro analogues of **3** by TxtA, TxtB, and TCB14. A) TCB14 hydroxylated desnitro-4Me-thaxtomin D (**7**) was synthesized with TxtA and TxtB (1.2 μM) after 30 h (trace II) and showed the same retention time as that of the standard (trace III). Trace I showed the reaction of TCB14 with mono- and dihydroxylated **7**, as indicated by Δ and #, respectively. B) TCB14 hydroxylated 28 of the 30 desnitro analogues of **3** synthesized from 5 L-Trp and 6 L-Phe analogues, with conversion ratios ranging from 40.0 to 0.2%. The products were detected at 280 nm by HPLC and their concentrations were then determined by using the standard curve of cyclo-(L-Trp-L-Phe). The conversion ratios of mono- and dihydroxylated products are shown as solid and sliced bars, respectively. The data represent means of at least two independent experiments, with details shown in Table S2.

that the C4-NO₂ group of thaxtomins is dispensable to the TCB14 reaction. This result was supported by a recent *in vivo* study in which TxtC was heterologously expressed in *S. albus* and converted the majority of *in situ* generated **7** mainly into the monohydroxylated product (about 0.1 mg L⁻¹).^[23a] The observed product profile difference of the *in vitro* and *in vivo* TxtC reactions can be related to substrate availability.

To further evaluate the substrate requirement of TCB14, we prepared a library of 30 desnitro analogues of **3**, including **7** in the TxtA and TxtB reactions with five L-Trp (L-Trp, 4Me-D,L-Trp, 4F-L-Trp, 5F-L-Trp, and 6F-D,L-Trp; 0.5 mM) and six L-Phe (L-Phe, 2F-L-Phe, 3F-L-Phe, 3Cl-L-Phe, 4F-L-Phe, and 4Cl-L-Phe; 0.5 mM) analogues as substrates.^[21a] Notably, only the L-form of racemic amino acids is taken for the enzymatic DKP synthesis.^[21a] In our recent work, the conversion ratios of this library varied from 22 to 0.7%, making the calculated concentrations of potential TCB14 substrates as low as 3.5 μM .^[21a] To enhance substrate availability for TCB14 reactions, we doubled the concentrations of both TxtA and TxtB (2.4 μM) for library preparation. We then incubated TCB14 at 3.0 μM with this library for 20 h. Notably, the TxtA and TxtB reactions were not terminated upon adding TCB14 and likely continued. HPLC analysis of the one-pot, three-enzyme reactions revealed that 28 out of 30

desnitro analogues of **3** were converted into a total of 43 mono- or dihydroxylated products (Figure 3B). Hydroxylated products were confirmed by HRMS and tandem MS/MS analyses (Figure S5 and Table S2). We then determined the concentrations of hydroxylated products by using the standard curve of commercially available cyclo-(L-Trp-L-Phe). The conversion ratios of the TxtA, TxtB, and TCB14 reactions were calculated as [hydroxylated product]/0.5 mM × 100% and ranged from 40.0 to 0.2% (Table S2). Undetectable amounts of hydroxylated products were available in the reaction with 4F-L-Trp and 3F-L-Phe or 6F-D,L-Trp and 3Cl-L-Phe as substrates (Figure 3B). TCB14 tended to be more active toward the substrates constructed from 4Me-L-Trp. Indeed, the three best enzyme substrates were **7**, desnitro-4Me-19F-thaxtomin D, and desnitro-4Me-20F-thaxtomin D, the conversion ratios of which were all about 40% (Figure 3B). Compared with the -F substituent on the C3 and C4 atoms of the phenyl group of L-Phe, the replacement of -Cl significantly reduced the conversion ratios of TCB14 toward the DKPs with 4Me-L-Trp as the other building block. On the other hand, TCB14 showed low conversion ratios (4.8 to 0.2%) toward other 23 desnitro DKP substrates (Figure 3B and Table S2). Another observation was that TCB14 produced more dihydroxylated products than those with a single -OH group (27 vs. 16). The conversion ratios of dihydroxylation were also higher in 23 of 28 TCB14 reactions. Notably, TCB14 produced dihydroxylated products from eight desnitro DKP substrates constructed from 3F-L-Phe and 3Cl-L-Phe; thus suggesting that TCB14 is able to hydroxylate the alternative site of the phenyl group if C20 is occluded. The regiospecificity of enzymatic aromatic hydroxylation was further highlighted by the production of one major and one minor dihydroxylated products from desnitro thaxtomin D; desnitro-20F-thaxtomin D; and five desnitro analogues of **3** that comprise 4Me-L-Trp and L-Phe, 2F-L-Phe, 3F-L-Phe, 4F-L-Phe, and 4Cl-L-Phe as the other building block (Table S2). In line with this observation, our recent study found that TCB14 produced dihydroxylated products from analogues of **3**, the C20 sites of which were substituted with -F, -Cl, or -Br.^[21a] The alternative hydroxylation site can be *ortho* to the methylene group, followed by *para*-hydroxylation, as suggested by recent studies from the groups of Micklefield and Challis.^[23a,24] Collectively, the present study revealed the considerable promiscuity of TCB14 in hydroxylating desnitro analogues of **3**, particularly those with small substituents on the C4, C5, C19, and C20 sites. These hydroxylated products can be used to develop new herbicides, for example, gaining insights into the structure-activity relationship. Indeed, our recent study revealed the potent herbicidal activity of compound **7**.^[21a] Among all substituents, the C4-CH₃ group gave rise to higher conversion ratios likely due to its efficient interactions with a hydrophobic nitro-binding cavity in the TxtC active site.^[24] On the other hand, we are aware that the uneven abundance of desnitro analogues of **3** synthesized in the TxtA and TxtB reactions can influence the TCB14 reactions. For example, **7** and desnitro-4Me-20F-thaxtomin D are the two most abundant products of the library of desnitro analogues of **3** in our recent study.^[21a] However, the substrate concentration is not the sole determining factor of

the catalytic performance of TCB14. Indeed, although TxtA and TxtB showed similar levels of conversion ratios toward 5F-L-Trp and 4Me-L-Trp,^[21a] the six DKPs with 5F-L-Trp as one building block had conversion ratios ranging from only 3.9 to 0.4% (Figure 3B, Table S2).

Multiple hydroxylated, methylated, aromatic DKPs produced in one-pot reactions with TCB14 and Amir_4628

With an advanced understanding of TCB14 promiscuity, we attempted to employ this enzyme to hydroxylate aromatic DKPs that were structurally different from desnitro thaxtomins. We selected ten commercially available aromatic DKPs for this study (Figure S8), all of which contained at least one aromatic amino acid building block. Given the strong preference of TCB14 toward the substrates with two DKP N-CH₃ groups (Figure 2), we next selected Amir_4628 to methylate these select aromatic DKPs.^[30] Amir_4628 is a relatively promiscuous N-MT enzyme of the actinobacterium *Actinosynnema mirum* and generates mono- and/or di-N-methylated cyclo-(L-Trp-L-Trp), named cWW-Me and cWW-Me₂, respectively. This enzyme also methylates four other L-Phe containing DKPs, cFF, cFY, cFM, and cFL, with reduced efficiency.^[30] We expressed the codon-optimized *Amir_4628* gene in *E. coli* and prepared the recombinant enzyme (Figures S1 and S9).^[30] Furthermore, the human *hMAT2A* cDNA was expressed in *E. coli* to obtain the enzyme for generating SAM from L-Met and ATP (Figure S1), thereby reducing the reaction cost.^[31] In the proof-of-concept study, we incubated cWF with Amir_4628 and hMAT2A or SAM for 20 h. To our delight, HPLC analysis revealed that about (57.7 ± 4.7)% of cWF was converted into cWF-Me₂ with a small quantity of cWF-Me ((2.2 ± 1.4)%; traces II and III, Figure 4A). These products showed the expected *m/z* values by HRMS analysis and their tandem MS patterns suggested that mono-methylation occurred on the amine group of L-Phe (Figures S5 and S10). Both SAM and hMAT2A were equally efficient in supporting the reaction. Subsequently, we added TCB14 to the above reaction mixture. After 20 h, HPLC analysis showed the complete conversion of cWF-Me₂ into mono- (67%) and dihydroxylated (33%) products (trace IV, Figure 4A). The products showed the expected *m/z* values in HRMS analysis and tandem MS patterns (Table S3). Intriguingly, two dihydroxylated products with retention times of 8.8 and 9.6 min were produced in the reaction; thus further illuminating the regiospecificity of TCB14. Collectively, these results demonstrated the successful development of the biocatalytic route to hydroxylated desnitro thaxtomin analogues starting from cWF.

Next, we employed the above biocatalysis strategy to hydroxylate nine other aromatic DKPs (Figure S8). HPLC and HRMS analysis revealed that Amir_4628 methylated five DKPs to a varying extent (Figure 4B and Table S3); cPH, cGF, cSF, and brevianamide F (cPW) were not methylated. The location of the single methyl group on the DKPs, except cGW, was determined on the basis of tandem MS analysis (Table S3).^[21a,30] Amir_4628 converted about 69.5% of the best substrate, cWW, into (47.2 ± 5.0)% of cWW-Me₂ and (22.3 ± 3.5)% of cWW-Me (Figure 4B). The other top substrates included cWY, cLF, and

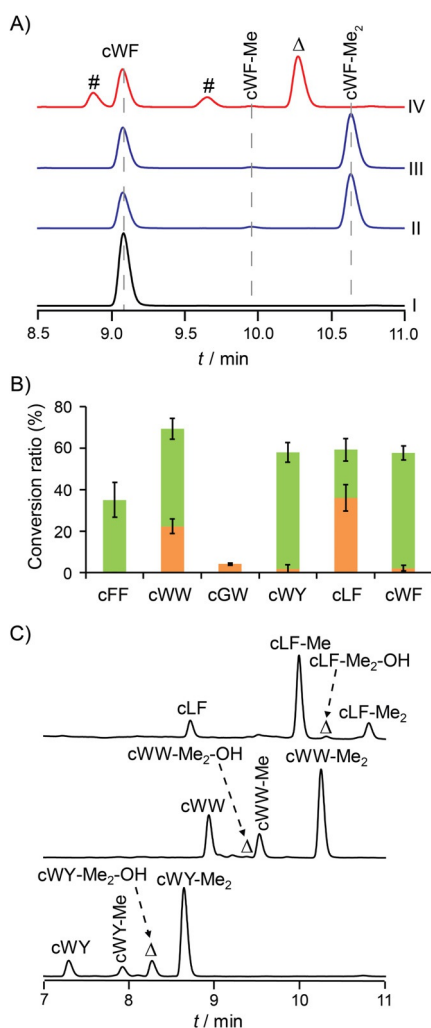


Figure 4. Biocatalytic synthesis of hydroxylated, methylated, aromatic DKPs by using TCB14 and Amir_4628. A) HPLC analysis revealed the formation of methylated cWFs and hydroxylated cWF-Me₂. Trace I represents the negative control containing heat-inactivated Amir_4628, whereas traces II and III show the full reactions with SAM or hMAT2A that generate SAM in situ, respectively. Trace IV indicates the above reaction after adding TCB14. The peaks of mono- and dihydroxylated cWF-Me₂ are indicated with Δ and #, respectively. B) Amir_4628 methylated six aromatic DKPs to a varying extent. Mono- and dimethylated products are shown as orange and green bars, respectively. The complete consumption of DKP substrates was set as 100% of the conversion ratio. The data represent means \pm s.d. of at least two independent experiments. C) HPLC analysis revealed that TCB14 was able to produce monohydroxylated cWW-Me₂, cWY-Me₂, and cLF-Me₂, as indicated by Δ .

cWF; all of which were converted by about 58%. On the other hand, cGW was a poor substrate of Amir_4628 with 4.3% conversion into cGW-Me (Figure 4B). Interestingly, the single product from cFF was cFF-Me₂ (about 35% conversion), which demonstrated a different product profile than that of the previous in vivo study.^[30] With an advanced understanding of the methylated DKP profiles of the Amir_4628 reaction, we then sought to hydroxylate methylated DKPs by using TCB14. Notably, Amir_4628 was likely to continue its reaction after the addition of TCB14 (Figure 4B and C). HPLC, HRMS, and tandem MS analyses showed the production of monohydroxylated

cWY-Me₂, cWW-Me₂, and cLF-Me₂, but the conversion ratios were low (Figure 4C and Table S3). Collectively, this work indicates that TCB14 is able to hydroxylate DKP scaffolds carrying at least one aromatic amino acid building block, and future engineering can make this enzyme more useful to synthetic applications. Similar to TCB14, both CYP121 and CYP134A1 act on unnatural DKP substrates to varying extents in in vitro studies.^[27b,28]

Conclusions

Both aliphatic and aromatic C–H hydroxylations are synthetically useful reactions. We characterized, in detail, the substrate requirement of TCB14 and employed it, along with TxtA and TxtB or Amir_4628, to produce over 40 novel hydroxylated, methylated, aromatic DKPs. Our study revealed that both N12– and N15–CH₃ of thaxtomin analogues were essential to efficient hydroxylation by TCB14, while the enzyme showed potential for hydroxylating substrates carrying small substituents on the indole and phenyl moieties, including omission of the C4–NO₂ group. Finally, the use of Amir_4628^[30] and TCB14 successfully produced monohydroxylated and dimethylated cWWs, cWYs, and cLFs, albeit with low conversion ratios. The formation of cLF-Me₂-OH further highlights the significant promiscuity of TCB14 toward aromatic DKP-Me₂ substrates; thus suggesting its potential for synthetic applications. Future studies will improve the catalytic performance (e.g., coupling efficiency) of TxtC biocatalysts. Encouragingly, during the review of the present work, the group of Challis reported the rapid conversion of **3** into **2** and then **1** by TxtC reconstituted with spinach ferredoxin and ferredoxin reductase,^[24] which suggested the evaluation of additional redox partners for creating more active, self-sufficient biocatalysts.^[34] Furthermore, the crystal structures of TxtC can aid engineering efforts to develop biocatalysts for hydroxylating structurally diverse aromatic DKPs. It is also envisioned that other functionally diverse enzymes (e.g., O-prenyltransferases) from different sources^[35] can be incorporated to expand the structural and functional spectra of hydroxylated aromatic DKPs.

Experimental Section

General: Molecular biology reagents and chemicals were purchased from Fisher Scientific, Sigma-Aldrich, or New England Biolabs, Inc, unless specified otherwise. Primers were ordered from Sigma-Aldrich. 4-Me-D,L-tryptophan was from MP Biomedical (Santa Ana, CA), whereas 3-(aminopropyl)-1-hydroxy-3-isopropyl-2-oxo-1-triazene (NOC-5) was purchased from EMD Millipore. Nine cyclic dipeptides used in this study were purchased from ChemImpex Int'l, Inc. Brevianamide F was purchased from Ark Pharm, Inc. *E. coli* BL21-GOLD (DE3; Agilent) and BAP1 were used for routine molecular biology studies (Table S4) and protein expression, respectively, and were grown in lysogeny broth or Terrific broth. DNA sequencing was performed at Eurofins. Primers used in this study are listed in Table S5. TB14 used in the study was reported in our previous study.^[32] 1D and 2D NMR spectra of compounds were recorded in CD₃OD on a Bruker 600 MHz spectrometer by using the 1.5 mm high-temperature superconducting cryogenic probe at

the University of Florida, Gainesville, FL, USA. Spectroscopy data were collected by using Topspin 3.5 software. All ^1H NMR were water suppressed to remove the high background water signal. HRMS data were obtained by using a Thermo Fisher Q Exactive Focus mass spectrometer equipped with an electrospray probe on a Universal Ion Max API source.

Enzyme preparation: The plasmids of TCBXs were prepared by following the same method for constructing TCB14.^[21a] Briefly, the *txtC* gene was amplified from pET26b-TCB14 in the PCR reaction by using a pair of primers, C-NcoI-F and C-SacI-R (Table S5). The PCR product was purified and digested with the restriction enzymes NcoI and SacI. pET28b-TB11, TB17, and TB22 vectors that we prepared previously^[32] were digested with the above two enzymes and the linear plasmids were purified. The digested *txtC* fragment was then ligated with the corresponding digested plasmids to generate expression constructs pET28b-TCBXs. For the expression of Amir_4628, codon-optimized Amir_4628 was used as a template for PCR amplification. To obtain the TxB mutant G554R, primers carrying the mutation site were used to amplify two fragments in the PCR reactions with pET28b-TxB as a template. After purification, the two fragments were assembled by using the Gibbon assembly method (New England Biolabs). Inserts in all expression constructs were sequenced to exclude any potential errors introduced during PCR amplification and gene manipulation. *E. coli* transformation, protein expression, and purification followed our previously established protocols.^[32] Briefly, *E. coli* cells harboring the expression constructs were cultured in Terrific broth medium supplemented with suitable antibiotics at 37 °C, 250 rpm. To express P450s, the medium also contained 1 × trace metal solution (1000 × stock solution: 50 mM FeCl₃, 20 mM CaCl₂, 10 mM MnSO₄, 10 mM ZnSO₄, 2 mM CoSO₄, 2 mM CuCl₂, 2 mM NiCl₂, 2 mM Na₂MoO₄, and 2 mM H₃BO₃). After OD₆₀₀ reached 0.6, protein expression was induced with isopropyl β-D-1-thiogalactopyranoside (IPTG; 0.1 mM) at 16 °C, 250 rpm for 16 h. Cell pellets were then collected after centrifugation (5000g, 10 min, and 4 °C). To purify recombinant proteins, cell pellets were resuspended in lysis buffer (cell biomass/volume = 1:4; 25 mM Tris-HCl, pH 8.0, 100 mM NaCl, 20 mM imidazole, 3 mM β-mercaptoethanol, and 10% glycerol). Soluble proteins were released by sonication and collected by centrifugation at 35000g at 4 °C for 30 min. Ni-NTA agarose resin (Thermo) was then used for protein purification. Purified recombinant proteins were exchanged into a storage buffer (25 mM Tris-HCl, pH 8.0, 100 mM NaCl, 3 mM βME, and 10% glycerol) by using a PD-10 column, aliquoted, and stored at -80 °C until required. Protein concentrations were determined by NanoDrop, whereas the concentrations of properly folded TCBXs were measured by absorbance difference at two wavelengths of $\lambda \approx 420$ nm and 390 nm after differential CO-reduced P450 spectral analysis.^[32]

Enzyme reactions: The TCB14 reaction solutions (100 mM Tris-Cl, pH 8.0, 100 μL) typically contained compound 3–7 or other substrates (0.1–0.2 mM) and the NADPH regeneration system (9.0 μM GDH, 0.75 mM NADPH, and 30.0 mM glucose). The reactions were initiated by adding TCB14 (1.5–15.0 μM final concentration) and incubated at 21 °C, 400 rpm, for 2–20 h prior to termination with methanol (200 μL). The resulting mixtures were centrifuged at 18407g for 15 min and clear supernatant (10 or 20 μL) was then subjected to HPLC analysis. One-pot biocombinatorial synthesis of hydroxylated desnitro analogues of 3 comprised two stages, including the first step for the production of desnitro 3 with TxtA and TxtB (2.4 μM, 21 °C, 400 rpm for 30 h), and the second step driven by TCB14 (3.0 μM) and the GDH system (21 °C, 400 rpm for 20 h). The products were analyzed and quantitated by HPLC and

LC-MS analyses. The Amir_4628 reaction solutions (100 mM Tris-Cl, pH 8.0, 200 mM NaCl, 100 μL) typically contained DKP (0.5 mM) and SAM (2.5 mM). Alternatively, the reactions contained the SAM generation system (8.6 μM hMAT2A, 5 mM ATP, 1 mM MgCl₂, 100 mM KCl, and 2.5 mM L-methionine). The reactions were initiated by adding Amir_4628 (67.0 μM final concentration) and incubated at 21 °C, 400 rpm for 20 h prior to termination with methanol (200 μL). The resulting mixtures were centrifuged at 18407g for 15 min and then clear supernatant (10 μL) was subjected to HPLC analysis. The coupling reaction (50 mM Tris-Cl, pH 8.0, 100 mM NaCl, 100 μL) of Amir_4628 with TCB14 typically contained Amir_4628 (38.5 μM), TCB14 (15.0 μM), the NADPH regeneration system, DKPs (0.25 mM), SAM (1.25 mM for cWW and cLF), or the SAM generation system (cWF and cWY). The reactions were incubated at 21 °C, 400 rpm, for 20 h prior to termination with methanol (200 μL). The resulting mixtures were centrifuged at 18407g for 15 min and then clear supernatant (10 μL) was subjected to HPLC analysis. All experiments were repeated independently at least twice.

Determination of conversion ratios: The quantitation of thaxto-min analogues in the enzymatic reactions were based on the standard curve of 1. The quantitation of hydroxylated desnitro DKPs in the TxtA, TxtB, and TCB14 reactions was based on the standard curve of cWF. The conversion ratios into hydroxylated products were calculated as [hydroxylated product]/0.5 mM × 100%. The conversion ratios of methylation and hydroxylation of aromatic DKPs were based on the comparison of UV trace integrals of products areas to the total areas of the UV trace integrals of both the substrate and products.

Large-scale enzymatic synthesis of DKP analogues: The enzymatic syntheses of compounds 5 and 6 were based on our previous study,^[21a] except TxB G554R, which was used for the synthesis of compound 6.

Determination of binding affinities between substrates and TCB14: The ForteBio Octet RED384 System equipped with ForteBio Dip and ReadTM Anti-Penta-HIS1K (HIS1K) biosensors was used to quantitate the binding between TCB14 and compounds 3–6. This technique measured the interaction kinetics of small molecules and biomolecules through recording changes of the interference pattern of white light, which was reflected from a layer of immobilized partner on the biosensor tip. The biosensors were hydrated in desalting buffer (pH 8.0) for 10 min prior to experiments. TCB14 (100 μg mL⁻¹) was reconstituted in desalting buffer. The gradient concentrations of analytes were 1000, 200, 40, 8, 1.6, and 0.32 μM. The time scheme setting was as follows: an initial baseline for 200 s, loading for 900 s, baseline for 600 s, association for 900 s, and dissociation for 900 s. Correction of baseline drift was performed by subtracting the averaged shift recorded for a sensor loaded with TCB14, but incubated with desalting buffer. Experimental data were fitted by using a global fit 1:1 model to determine the K_d values. The binding affinity of 3 with TCB14 was further determined by using the UV-titration method.^[32] The stock solution of 3 (10 mM) was prepared in DMSO. Serial volumes (0–10 μL, 1 μL each time) of the stock solution were then added to TCB14 solution (1.5 μM) to record the spectra. Blank controls were buffers containing the corresponding volumes of the stock solution because 3 had a maximal absorbance at $\lambda = 380$ nm. The changes in absorbance (ΔA) were then determined by subtracting the absorbance at $\lambda \approx 420$ nm from that at $\lambda \approx 392$ nm. Data were then fitted to the equation $\Delta A = \Delta A_{\text{max}}[L]/(K_d + [L])$ by using GraphPad Prism 4.

Spectral analysis of TCBX: The absorbance spectra ($\lambda = 400\text{--}600\text{ nm}$) of the recombinant enzymes in Tris-HCl (25 mM, pH 9) buffer were recorded by using a Shimadzu UV2700 dual beam UV/Vis spectrophotometer. The ferric heme of the enzymes was then saturated by gentle bubbling of carbon monoxide (Airgas) for 1 min, and the spectra of enzyme solutions were then recorded. A finite amount of solid sodium dithionite (Fisher) was subsequently added to enzyme solutions to reduce the ferric heme. After recording the reduced spectra, we generated the CO-reduced differential spectra of all enzymes by subtracting their CO binding spectra from the corresponding reduced spectra. Data were further plotted in Excel.

Determination of the coupling efficiency of TCBXs: To determine the coupling efficiency, the reaction mixtures contained TCBX (1.5 μM), **3** (0.1 mM), and NADPH (0.4 mM), and were incubated at 24 °C for 30 min. NADPH consumption was measured at $\lambda = 340\text{ nm}$ ($\epsilon = 6.22\text{ mm}^{-1}\text{ cm}^{-1}$) with a Biotek Synergy HT multidetection microplate reader. Non-enzymatic oxidation of NADPH was subtracted as the background. The amount of hydroxylated product was determined by HPLC analysis. Coupling efficiency [%] was determined as product [nmol]/consumed NADPH [nmol] $\times 100\%$. All reactions were repeated independently at least three times.

Acknowledgements

We thank Jim Rocca, Prof. Eric W. Schmidt (University of Utah), Prof. Steven D. Bruner, Chao Xie, and Peilan Zhang for technical assistance. NMR spectra were recorded at the AMRIS facility at UF with support from an NHMFL grant (ML-Ding-001). The AMRIS facility was supported by the National Science Foundation (DMR-1157490 and DMR-1644779) and the State of Florida. The 1.5 mm high-temperature superconducting cryogenic probe was developed with support from NIH Award R01EB009772. This study was partially supported by the University of Florida Opportunity Fund (Y.D., R.L.) and UF Emerging Scholar and University Scholar programs (M.P.). Y.D. is an Air Force Office of Scientific Research Young Investigator (FA9550-16-1-0186).

Conflict of Interest

The authors declare no conflict of interest.

Keywords: biocatalysis • cytochromes • enzymes • hydroxylation • structure–activity relationship

- [1] a) M. Parvez, L. B. Qhanya, N. T. Mthakathi, I. K. Kgosiemang, H. D. Bamal, N. S. Pagadala, T. Xie, H. Yang, H. Chen, C. W. Theron, R. Monyaki, S. C. Raselemane, V. Salewe, B. L. Mongale, R. G. Matowane, S. M. Abdalla, W. I. Booi, M. van Wyk, D. Olivier, C. E. Boucher, D. R. Nelson, J. A. Tuszyński, J. M. Blackburn, J. H. Yu, S. S. Mashela, W. Chen, K. Syed, *Sci. Rep.* **2016**, *6*, 33099; b) J. D. Rudolf, C. Y. Chang, M. Ma, B. Shen, *Nat. Prod. Rep.* **2017**, *34*, 1141–1172.
- [2] a) F. P. Guengerich, *Chem. Res. Toxicol.* **2001**, *14*, 611–650; b) X. Zhang, S. Li, *Nat. Prod. Rep.* **2017**, *34*, 1061–1089.
- [3] a) I. G. Denisov, T. M. Makris, S. G. Sligar, I. Schlichting, *Chem. Rev.* **2005**, *105*, 2253–2277; b) C. M. Krest, E. L. Onderko, T. H. Yosca, J. C. Calixto, R. F. Karp, J. Livada, J. Rittle, M. T. Green, *J. Biol. Chem.* **2013**, *288*, 17074–17081; c) P. R. Ortiz de Montellano, *Chem. Rev.* **2010**, *110*, 932–948; d) P. J. Mak, I. G. Denisov, *Biochim. Biophys. Acta Proteins Proteomics* **2018**, *1866*, 178–204.
- [4] a) F. P. Guengerich, A. W. Munro, *J. Biol. Chem.* **2013**, *288*, 17065–17073; b) J. Rittle, M. T. Green, *Science* **2010**, *330*, 933–937.
- [5] a) S. Sivaramakrishnan, H. Ouellet, H. Matsumura, S. H. Guan, P. Moenne-Loccoz, A. L. Burlingame, P. R. O. de Montellano, *J. Am. Chem. Soc.* **2012**, *134*, 6673–6684; b) M. J. Cryle, J. J. De Voss, *Angew. Chem. Int. Ed.* **2006**, *45*, 8221–8223; *Angew. Chem.* **2006**, *118*, 8401–8403; c) S. X. Jin, T. M. Makris, T. A. Bryson, S. G. Sligar, J. H. Dawson, *J. Am. Chem. Soc.* **2003**, *125*, 3406–3407.
- [6] a) G. Saab-Rincón, H. Alwaseem, V. Guzmán-Luna, L. Olvera, R. Fasan, *ChemBioChem* **2018**, *19*, 622–632; b) H. M. Girvan, A. W. Munro, *Curr. Opin. Chem. Biol.* **2016**, *31*, 136–145; c) R. K. Zhang, X. Huang, F. H. Arnold, *Curr. Opin. Chem. Biol.* **2019**, *49*, 67–75; d) Y. Wei, E. L. Ang, H. Zhao, *Curr. Opin. Chem. Biol.* **2018**, *43*, 1–7.
- [7] a) L. Katz, R. H. Baltz, *J. Ind. Microbiol. Biotechnol.* **2016**, *43*, 155–176; b) D. J. Newman, G. M. Cragg, *J. Nat. Prod.* **2016**, *79*, 629–661; c) K. C. Nicolaou, *Proc. R. Soc. A* **2014**, *470*, 20130690.
- [8] a) H. Lachance, S. Wetzel, K. Kumar, H. Waldmann, *J. Med. Chem.* **2012**, *55*, 5989–6001; b) C. R. Pye, M. J. Bertin, R. S. Lokey, W. H. Gerwick, R. G. Lington, *Proc. Natl. Acad. Sci. USA* **2017**, *114*, 5601–5606.
- [9] A. Greule, J. E. Stok, J. J. De Voss, M. J. Cryle, *Nat. Prod. Rep.* **2018**, *35*, 757–791.
- [10] a) Y. Q. Xue, D. Wilson, L. S. Zhao, H. W. Liu, D. H. Sherman, *Chem. Biol.* **1998**, *5*, 661–667; b) D. H. Sherman, S. Y. Li, L. V. Yermalitskaya, Y. C. Kim, J. A. Smith, M. R. Waterman, L. M. Podust, *J. Biol. Chem.* **2006**, *281*, 26289–26297.
- [11] J. C. Carlson, S. Y. Li, S. S. Gunatilleke, Y. Anzai, D. A. Burr, L. M. Podust, D. H. Sherman, *Nat. Chem.* **2011**, *3*, 628–633.
- [12] S. Uhlmann, R. D. Süßmuth, M. J. Cryle, *ACS Chem. Biol.* **2013**, *8*, 2586–2596.
- [13] T. Tokai, H. Koshino, N. Takahashi-Ando, M. Sato, M. Fujimura, M. Kimura, *Biochem. Biophys. Res. Commun.* **2007**, *353*, 412–417.
- [14] Q. F. Zheng, S. F. Wang, R. J. Liao, W. Liu, *ACS Chem. Biol.* **2016**, *11*, 2673–2678.
- [15] A. H. Payne, D. B. Hales, *Endocr. Rev.* **2004**, *25*, 947–970.
- [16] M. J. Cryle, I. Schlichting, *Proc. Natl. Acad. Sci. USA* **2008**, *105*, 15696–15701.
- [17] G. Jones, D. E. Prosser, M. Kaufmann, *Arch. Biochem. Biophys.* **2012**, *523*, 9–18.
- [18] a) A. Muliandi, Y. Katsuyama, K. Sone, M. Izumikawa, T. Moriya, J. Hashimoto, I. Kozono, M. Takagi, K. Shin-ya, Y. Ohnishi, *Chem. Biol.* **2014**, *21*, 923–934; b) A. W. Goering, R. A. McClure, J. R. Doroghazi, J. C. Albright, N. A. Haverland, Y. Zhang, K. S. Ju, R. J. Thomson, W. W. Metcalf, N. L. Kelleher, *ACS Cent. Sci.* **2016**, *2*, 99–108.
- [19] G. Guroff, J. W. Daly, D. M. Jerina, J. Renson, B. Witkop, S. Udenfriend, *Science* **1967**, *157*, 1524–1530.
- [20] R. Loria, D. R. Bignell, S. Moll, J. C. Huguet-Tapia, M. V. Joshi, E. G. Johnson, R. F. Seipke, D. M. Gibson, *Antonie Van Leeuwenhoek* **2008**, *94*, 3–10.
- [21] a) G. Jiang, R. Zuo, Y. Zhang, M. M. Powell, P. Zhang, S. M. Hylton, R. Loria, Y. Ding, *ACS Catal.* **2018**, *8*, 10761–10768; b) G. Jiang, Y. Zhang, M. M. Powell, P. Zhang, R. Zuo, Y. Zhang, D. Kallifidas, A. M. Tieu, H. Luesch, R. Loria, Y. Ding, *Appl. Environ. Microbiol.* **2018**, *84*, 00164-18.
- [22] S. Barry, J. Kers, E. Johnson, L. Song, P. Aston, B. Patel, S. Krasnoff, B. Crane, D. Gibson, R. Loria, G. Challis, *Nat. Chem. Biol.* **2012**, *8*, 814–816.
- [23] a) M. Winn, D. Francis, J. Micklefield, *Angew. Chem. Int. Ed.* **2018**, *57*, 6830–6833; *Angew. Chem.* **2018**, *130*, 6946–6949; b) F. G. Healy, S. B. Krasnoff, M. Wach, D. M. Gibson, R. Loria, *J. Bacteriol.* **2002**, *184*, 2019–2029.
- [24] L. M. Alkhalaf, S. M. Barry, D. Rea, A. Gallo, D. Griffiths, J. R. Lewandowski, V. Fulop, G. L. Challis, *J. Am. Chem. Soc.* **2019**, *141*, 216–222.
- [25] A. Ortiz, E. Sansinenea, *Curr. Med. Chem.* **2017**, *24*, 2773–2780.
- [26] a) A. Borthwick, *Chem. Rev.* **2012**, *112*, 3641–3716; b) H. Zhang, X. Ning, H. Hang, X. Ru, H. Li, Y. Li, L. Wang, X. Zhang, S. Yu, Y. Qiao, X. Wang, P. Wang, *Org. Lett.* **2013**, *15*, 5670–5673.
- [27] a) P. Belin, M. Le Du, A. Fielding, O. Lequin, M. Jacquet, J. Charbonnier, A. Lecoq, R. Thai, M. Courcon, C. Masson, C. Dugave, R. Genet, J. Pernolet, M. Gondry, *Proc. Natl. Acad. Sci. USA* **2009**, *106*, 7426–7431; b) M. Fonvielle, M. Le Du, O. Lequin, A. Lecoq, M. Jacquet, R. Thai, S. Dubois, G. Grach, M. Gondry, P. Belin, *J. Biol. Chem.* **2013**, *288*, 17347–17359.
- [28] M. J. Cryle, S. G. Bell, I. Schlichting, *Biochemistry* **2010**, *49*, 7282–7296.

- [29] S. Meng, W. Han, J. Zhao, X. Jian, H. Pan, G. Tang, *Angew. Chem. Int. Ed.* **2018**, *57*, 719–723; *Angew. Chem.* **2018**, *130*, 727–731.
- [30] T. Giessen, A. von Tesmar, M. Marahiel, *Biochemistry* **2013**, *52*, 4274–4283.
- [31] N. Shafqat, J. Muniz, E. Pilka, E. Papagrigoriou, F. von Delft, U. Oppermann, W. Yue, *Biochem. J.* **2013**, *452*, 27–36.
- [32] R. Zuo, Y. Zhang, C. Jiang, J. Hackett, R. Loria, S. Bruner, Y. Ding, *Sci. Rep.* **2017**, *7*, 842.
- [33] a) R. M. Kagan, S. Clarke, *Arch. Biochem. Biophys.* **1994**, *310*, 417–427; b) F. Yan, D. Auerbach, Y. Chai, L. Keller, Q. Tu, S. Hüttel, A. Glemser, H. A. Grab, T. Bach, Y. Zhang, R. Müller, *Angew. Chem. Int. Ed.* **2018**, *57*, 8754–8759; *Angew. Chem.* **2018**, *130*, 8890–8895.
- [34] W. Zhang, L. Du, F. Li, X. Zhang, Z. Qu, L. Hang, Z. Li, J. Sun, F. Qi, Q. Yao, Y. Sun, C. Geng, S. Li, *ACS Catal.* **2018**, *8*, 9992–10003.
- [35] a) M. Morita, Y. Hao, J. Jokela, D. Sardar, Z. Lin, K. Sivonen, S. Nair, E. Schmidt, *J. Am. Chem. Soc.* **2018**, *140*, 6044–6048; b) T. W. Giessen, M. A. Marahiel, *Front. Microbiol.* **2015**, *6*, 785.

Manuscript received: November 29, 2018

Accepted manuscript online: January 2, 2019

Version of record online: March 27, 2019
